2019-08-23

Dynamic Behaviors of FAGGBSHMNS Based Geopolymer Paste When Subjected to Impact Compressive Loadings

Dong, Z

10.1002/adem.201900621
Advanced Engineering Materials
Wiley

Advanced Engineering Materials
Accepted manuscript online: 23 August 2019
Manuscript accepted: 29 July 2019
Manuscript revised: 26 July 2019
Manuscript received: 23 May 2019
https://doi.org/10.1002/adem.201900621

Dynamic behaviors of FA-GGBS-HMNS based geopolymer paste when subjected to impact compressive loadings

Zhijun Dong[1], Aissa Bouaissi[2*], Xianfeng Wang[3], Yijiao Huang[3], Long-yuan Li[2], Mohd Mustafa Al Bakri Abdullah[4], Shamala Ramasamy[5]

1) Shenzhen Institute of Information Technology, Shenzhen Longxiang Road, Shenzhen, P. R. China (dongzj@sziit.edu.cn)
2) School of Engineering, University of Plymouth, Plymouth PL4 8AA, UK (aissa.bouaissi@plymouth.ac.uk, long-yuan.li@plymouth.ac.uk)
3) Guangdong Provincial Key Laboratory of Durability for Marine Civil Engineering, College of Civil and Transportation Engineering, Shenzhen University, Shenzhen, P. R. China (huangyj_civil@qq.com, xfw@szu.edu.cn)
4) Center of Excellence Geopolymer and Green Technology, Universiti Malaysia Perlis, Perlis 01000, Malaysia (mustafa_albakri@unimap.edu.my)
5) School of Materials Engineering, Universiti Malaysia Perlis, Perlis 01000, Malaysia ()
*Corresponding author.

Abstract – Reducing emission of CO_2 into the atmosphere is a challenge owing to rapid industrial development, particularly in developing countries. Ordinary Portland cement (OPC) is the second large consumed material just after water. It is estimated that the production of one ton OPC generates approximately 0.87 ton CO_2. Geopolymers are considered as the sustainable materials that possess similar or even better mechanical properties than OPC. Geopolymers are made from by-products such as fly ash, furnace slag and China clay. This paper reports an experimental study on the dynamic mechanical behaviors of FA-GGBS-HMNS based geopolymers when subjected to impact loading. The impact tests were performed using a split-Hopkinson pressure bar device. The test results show that both the dynamic compressive strength and ultimate strain of the FA-GGBS-HMNS based geopolymer paste increase with

increased strain rate. The failure modes were also found to be different in the specimens under different impact speeds.

Keywords: Impact; Strain rate; Geopolymer; Stress-strain equation; Split-Hopkinson pressure bar.

1. Introduction

In practical engineering, many structural materials may be subjected to impact loading and thus may undergo high strain rates. The dynamic strength of materials is one of the most important mechanical properties[1], which is needed for structure design against, for example, earthquakes and explosive loading[2]. Recently, geopolymers become popular because they have similar binder features as the ordinary Poland cement (OPC)[3,4], and thus are considered to be the replacement of OPC used in concrete. The raw materials used in the production of geopolymers are mostly industrial by-products, such as fly ash (FA), slags and metakaolin, which used to be treated as wastes and disposed by landfills. The use of these waste materials to produce geopolymers thus is very encouraged. In theory, any materials, which are rich in aluminosilicate contents, can be used as raw materials to produce geopolymers[5,6]. However, due to the variety in compositions in different raw materials the geopolymers formed from them may also have different mechanical properties. Therefore, it is important to study the mechanical and material properties of the geopolymers formed from different raw materials. Ground granulated blast-furnace slag (GGBS) is a by-product obtained from iron industries. It has been demonstrated that the use of GGBS in OPC concrete can improve the workability of fresh concrete, increase the strength and durability and decrease the long-term drying shrinkage of hardened concrete. High magnesium nickel slag (HMNS) is also an industrial by-product, produced from nickel production from high-magnesium nickel oxide ores. HMNS contains considerable amounts of silica, alumina and magnesium. Our previous study showed that the geopolymer, made from the combined FA, GGBS and HMNS, has better mechanical and material properties than those made by their individuals[7].

Most of existing studies on geopolymers were focused on the static properties of geopolymers and geopolymer concretes. There is lack of studies on the dynamic properties of geopolymer materials[8]. Research on OPC concrete has a long history, which involves both static and dynamic properties. For instance, Ficker[9] studied the quasi-static compressive strength of cement-based materials. His results showed that for wet cementitious materials their

compressive strength increases remarkably with the rate of quasi-static loading. Luo et al.[10] conducted the dynamic compressive tests of highly fluidized slag and FA based geopolymer concretes. Their results showed that there are strong correlations between the dynamic compressive strength and strain rate and between the energy absorption and stain rate. Gao et al.[11] examined the static and dynamic mechanical properties of alkali-activated slag concrete (AASC). The results showed that the AASC has a high dynamic compressive strength. Its peak toughness and energy absorption ability were also found to increase with the strain rate. The investigation into the effect of water immersion on the dynamic mechanical properties of geopolymer concrete[3] showed the similar findings where the dynamic compressive strength and impact toughness trend increased with the increase of strain rate, but the elastic modulus was found to be less sensitive to the strain rate. Many efforts have been made to identify the effect of water content in concrete on the dynamic mechanical properties[12,13] and on the strain-rate sensitivity of concrete materials[14,15]. Overall, it has been recognized that for cementitious materials there is a considerable difference between its static and dynamic properties[16,17], although some conflict results were reported in literature. For example, some researchers reported that the strain rate effect was more significant in high strength concrete[9], while in others the strain rate effect was not found to be substantial on the compressive strength[18].

Recently, Khandelwal et al.[19] investigated the effect of strain rate on the mechanical properties of FA-based geopolymer mortar under a dry condition. It was found that the mechanical properties of the geopolymer mortar have a logarithmical increase with the strain rate. Feng et al.[20] studied the effect of strain rate on the compressive strengths of both FA-based geopolymer mortar and geopolymer concrete by using Split-Hopkinson pressure bar (SHPB) technique. It was found that the alkaline activators have significantly influence on the quasi-static compressive strength of the geopolymer mortar and geopolymer concrete.

The literature survey described above shows that there are some studies on the dynamic properties of geopolymer materials, but most of them were focused on FA-based geopolymer mortar and/or geopolymer concrete[3,20]. In order to provide a better understanding of the dynamic behaviors of geopolymers made from different source materials, more work is needed. In this paper, an experimental study is presented on the impact behavior of FA-GGBS-HMNS based geopolymer paste when subjected to high strain rate compressive loadings. The experiments were performed by using a SHPB device[1,21]. The experimental results show that both the dynamic compressive strength and ultimate strain of the FA-GGBS-HMNS based

geopolymer paste increase with increased strain rate. The failure modes were also found to be different in the specimens under different impact speeds.

2. Experimental programme

Three sets of cylindrical specimens of FA-GGBS-HMNS based geopolymer paste were cast first. The diameters of the specimens in the three sets are 33 mm, 36 mm, and 37 mm, respectively. The raw materials used for the mix casting the geopolymer paste were FA (70% in mass), GGBS (20% in mass) and HMNS (10% in mass). The selection of the percentage on FA, GGBS and HMNS was based on our previous study on the static mechanical properties[7]. The FA used in the mix was the class F FA with a specific surface area of 1.3 m^2/g and an average particle size of around 17.37 μm. The GGBS used in the mix was common GGBS with a specific surface area of 0.106 m^2/g and an average particle size of approximately 138 μm. The HMNS used in the mix was obtained directly from Steel Plant in Shaanxi, China. The specific surface area and average particle size of the HMNS were about 0.0536 m^2/g and 280 μm, respectively. Table 1 shows the chemical compositions of FA, GGBS and HMNS used in the mix, which were determined by using X-ray fluorescence (XRF) spectroscopy.

The alkaline activators used in the mix are the sodium silicate (Na_2SiO_3) and sodium hydroxide (NaOH). The chemical compositions of the sodium silicate solution include Na_2O (14.7% in mass), SiO_2 (29.8% in mass) and water (55.5% in mass). The sodium hydroxide solution was prepared in the laboratory by dissolving sodium hydroxide pellets in water to make the solution of 12 M concentration. After cooling for 24 hours at room temperature, the sodium hydroxide solution was then mixed with the sodium silicate solution. The mass ratio of the two solutions (Na_2SiO_3/NaOH) used in the present study was 2.5. The mass ratio of the binder (FA-GGBS-HMNS) to the liquid (alkaline activators) was 2.0, which was chosen based on our previous studies[7]. Table 2 shows the mix design used for casting the FA-GGBS-HMNS based geopolymer paste specimens.

After the binders (FA, GGBS, HMNS) were completely mixed with the alkaline activators the formed fresh geopolymer paste was poured into the cylindrical molders of three different diameters. The cast specimens were demolded after 24 hours and then cured in the laboratory at the room temperature of 25±2ºC with a relative humidity of 85-90% before they were tested.

To implement the impact test at high strain rates, all specimens were cut into a disk shape with a thickness of 18 mm by using a diamond saw. Nine specimens from each set of an identical diameter were tested using three different impact speeds. For each impact speed three repeat tests were carried out. Thus, a total of 27 disk-shaped specimens were made and tested in the present study. The two surfaces on the two sides of the disk-shaped specimen were carefully polished and parallelized (see Figure 1). The impact tests were carried out using the SHPB advice, consisting of a gas gun, a striker bar, incident and transmitter bars as shown in Figure 2. The incident and transmitter bars used in SHPB are all made from the same alloy steel with high yield strength and have the same cross-section size. The length and diameter of them were 2000 mm and 40 mm, respectively. In order to reduce the friction between the geopolymer paste specimen and its two adjacent bars, a film of lubrication was used to coat the contact surfaces of its two adjacent bars. During the test, the striker bar, incident bar, disk-shaped specimen and transmitter bar were all centrally aligned in order to ensure the shock waves were propagated properly in the longitudinal direction. During the course of impact the stresses and strains occurred in both the incident and transmitter bars were remained in elastic range. To measure the incident, transmitted and reflected pulses, strain gauges were placed on both the incident and transmitter bars, which were recorded by a computer. According to the proportional relationship between the strain rate in the specimen and the elastic strains recorded in the incident and transmitter bars, the time-histories of the stress, strain, and strain rate occurring in the tested specimen can be obtained, from which a dynamic stress-strain constitutive equation can be achieved. In the present experimental study three impact speeds, 2 m/s, 4 m/s and 6 m/s were employed for the specimens in each set.

Table 1. Chemical compositions of FA, GGBS and HMNS

Composition	SiO_2	Al_2O_3	Fe_2O_3	CaO	TiO_2	SO_3	K_2O	MgO	MnO	P_2O_5	Na_2O	Cr_2O_3	LOI
FA	55.7	27.8	7.27	4.10	2.29	0.27	1.55	-	-	-	-	-	3.04
GGBS	28.2	9.73	0.98	52.7	1.01	1.46	1.22	2.90	0.74	-	-	-	3.76
HMNS	43.2	4.35	10.3	3.45	0.10	0.28	0.18	26.2	0.89	0.05	0.23	1.01	0.30

Note: The sum of listed elements is not up to 100. This is because some small mineral oxides such as ZnO, CuO, ZrO_2, etc., which have negligible influence on the properties of these materials, are not listed there.

Table 1. Mix design of FA-GGBS-HMNS based geopolymer paste

Materials	FA	GGBS	HMNS	Na_2SiO_3 solution	NaOH solution
Proportion (kg/m^3)	420	120	60	214.28	85.71

Figure 1. (a) Cutting machine. (b) Grinding equipment. (c) Specimen measurement.

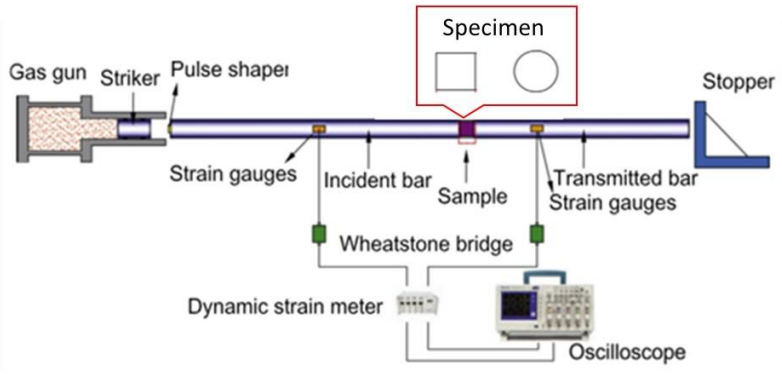

Figure 2. Schematic of Split-Hopkinson pressure bar system[16].

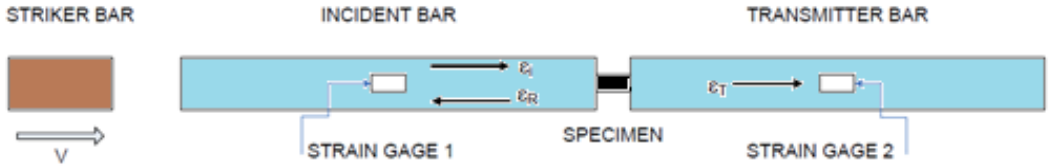

Figure 3. Specimen placed between incident and transmitter bars.

3. The principle of SHPB impact test

The principle of SHPB test is based on the one-dimensional elastic wave theory. By recording the strain histories on the incident and transmitter bars (see Figure 3), the strain rate, strain, and stress on the tested specimen can be calculated as follows[22]:

$$\dot{\varepsilon}(t) = -\frac{c_o}{l_o}(\varepsilon_i - \varepsilon_R - \varepsilon_T) \quad (1)$$

$$\varepsilon(t) = -\frac{c_o}{l_o}\int_o^t(\varepsilon_i - \varepsilon_R - \varepsilon_T)dt \quad (2)$$

$$\sigma(t) = \frac{EA}{2A_o}(\varepsilon_i + \varepsilon_R + \varepsilon_T) \quad (3)$$

where ε_i and ε_R are the incident and reflected strains recorded on the incident bar, ε_T is the transmitted strain recorded on the transmitter bar, $c_o = \sqrt{E/\rho}$ is the wave speed in the incident (or transmitter) bar, E, ρ, and A are the Young's modulus, density, and cross-sectional area of the incident (or transmitter) bar, A_o and l_o are the cross-sectional area and length of the tested specimen, respectively, $\dot{\varepsilon}(t)$, $\varepsilon(t)$ and $\sigma(t)$ are the average strain rate, average strain and average stress in the tested specimen. After the time-histories of the stress and strain are calculated using Eqs.(2) and (3) the dynamic stress-strain constitutive curve can be plotted by taking the time as an intermediate variant. The corresponding average strain rate of the obtained dynamic stress-strain curve can be calculated by using Eq.(1).

4. Results and discussions

In the SHPB impact test, the striker bar was boosted first by the gas pressure and the impact between the striker and incident bars generated a stress wave. This stress wave was propagated through the incident bar towards the specimen. When the stress wave reached the specimen, part of it was transmitted through the transmitter bar, and another part was reflected back to the incident bar. Figure 4 shows the typical waves of the incident, transmitted and reflected pulses recorded in the incident and transmitter bars during one of the tests. The voltage recorded in the data file was converted into the strain through an equivalent calibration test and thus its value is directly proportional to the strain. It can be seen from the figure that the amplitude of the incident pulse is larger than that of the transmitted or reflected pulse, indicating that some of the kinetic energy was absorbed by the tested specimen during the wave propagation. Also, it can be observed from the figure that the width of the transmitted pulse is wider than that of

the incident pulse and the amplitude of the reflected pulse decreases with time. The former indicates that the tested specimen has a viscosity feature; whereas the latter implies that the tested specimen exhibits a large plastic deformation. The time-histories of these recorded pulses were further used to calculate the time-histories of the strain rate, strain and stress of the specimen using Eqs.(1)-(3), from which the stress-strain curve of the tested specimen was obtained for that impact test.

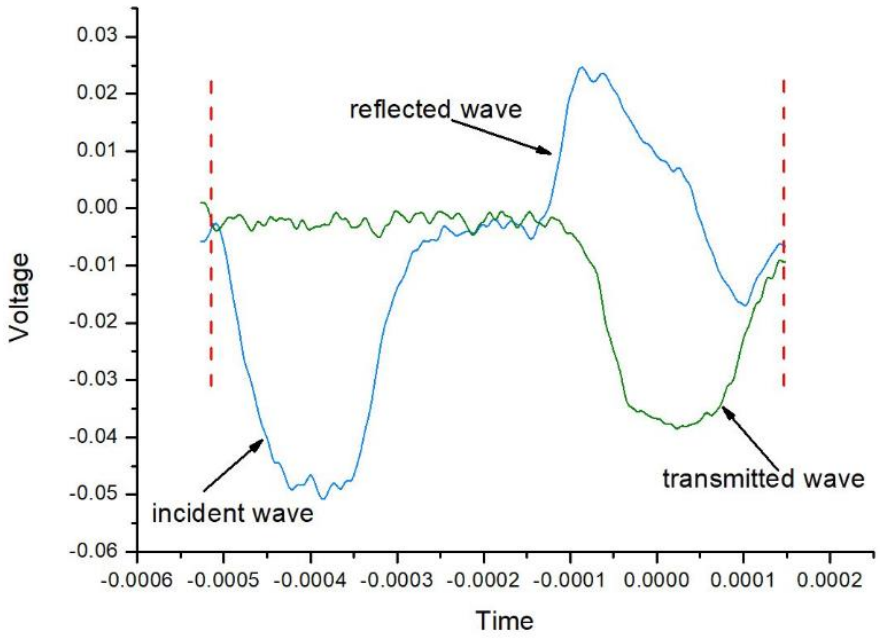

Figure 4. Incident, transmitted and reflected pulses recorded in an impact test.

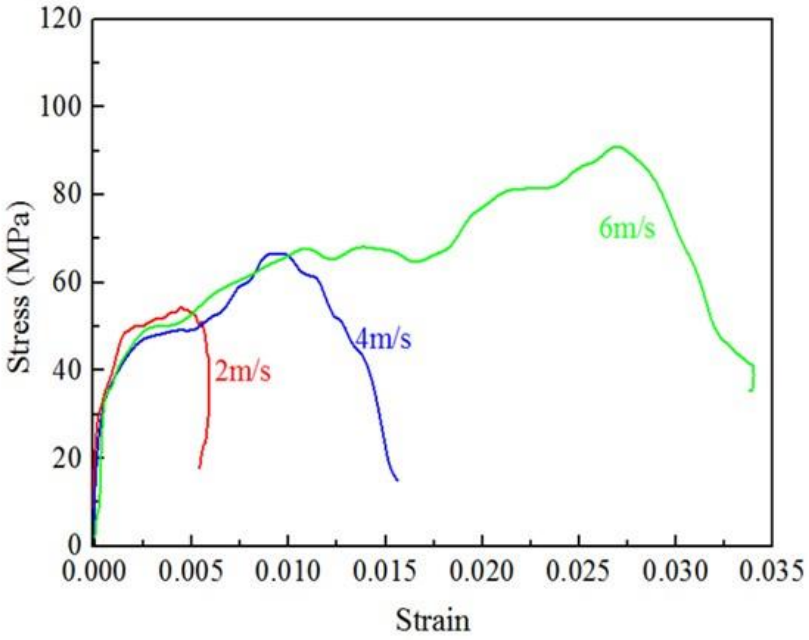

Figure 5. Dynamic stress-strain curves of FA-GGBS-HMNS based geopolymer pastes (group of set one with diameter 33 mm).

Figure 5 shows the dynamic compressive stress-strain curves of the three FA-GGBS-HMNS based geopolymer paste specimens in the group of set one (d = 33 mm) under three different impact speeds. It can be seen from the figure that, the three dynamic stress-strain curves have a similar variation pattern, in which the stress firstly has a fast increase almost linearly with the strain representing the elastic relationship between the stress and strain, then it has a slow improvement with the increased strain representing the feature of strain hardening, and finally after the stress reaches to a ultimate value it drops rapidly representing the compression failure of the specimen. It seems that the yield stress of the tested specimens did not change a lot when the impact speed was changed. However, the ultimate compressive strength of the specimens was found to increase with the increased impact speed. For example, the ultimate strength of the three specimens shown in Figure 5 are 55 MPa, 67 MPa and 90 MPa for the impact speed of 2 m/s, 4 m/s and 6 m/s, respectively. This implies that the FA-GGBS-HMNS based geopolymer paste is a strain rate-sensitive material. In addition, it was found that the impact speed had a significant influence on the ductility of the FA-GGBS-HMNS based geopolymer paste. The larger the impact speed, the wider the strain hardening zone. For example, the ultimate strain of the FA-GGBS-HMNS based geopolymer paste was found to be 0.005, 0.008, and 0.027, for the impact speed of 2 m/s, 4 m/s and 6 m/s, respectively, indicating that it has an exponential increase with the impact speed.

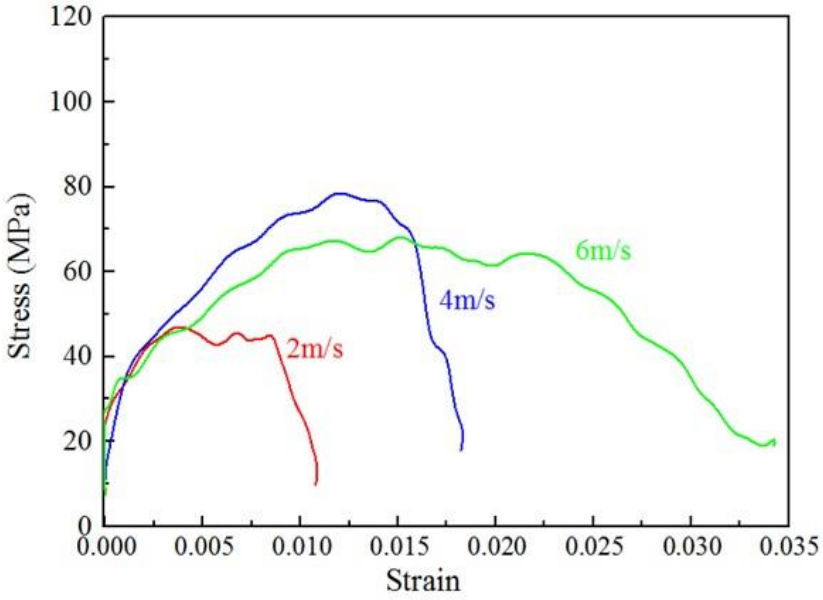

Figure 6. Dynamic stress-strain curves of FA-GGBS-HMNS based geopolymer pastes (group of set two with diameter 36 mm).

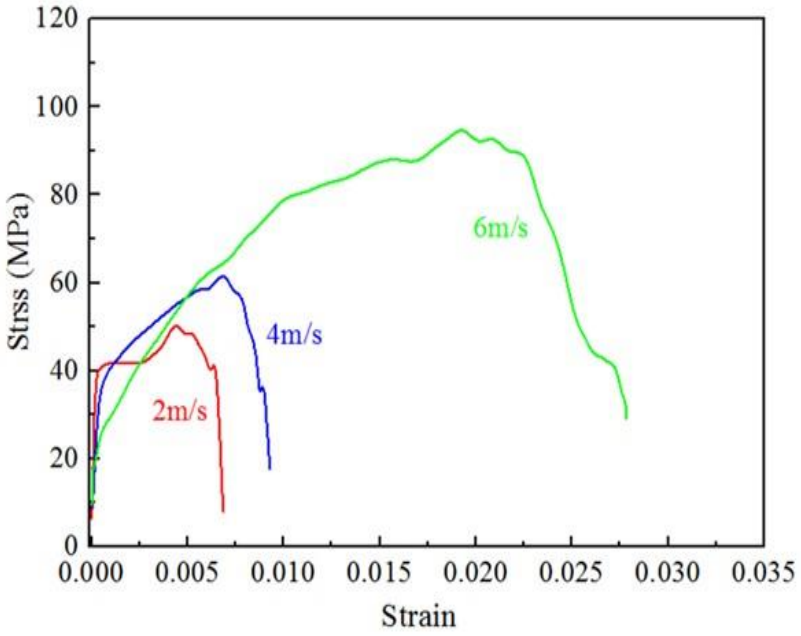

Figure 7. Dynamic stress-strain curves of FA-GGBS-HMNS based geopolymer pastes (group of set three with diameter 37 mm).

Figures 6 and 7 show the dynamic compressive stress-strain curves of the FA-GGBS-HMNS based geopolymer paste specimens in the groups of set two (d=36 mm) and set three (d=37 mm) under three different impact speeds. The main features observed from these two figures

are similar to those shown in Figure 5, except for that the ultimate strength in the curve of impact speed 6 m/s in the group of set two is lower than that in the curve of impact speed 4 m/s. This is probably due to the random mix and curing of the geopolymer materials. Nevertheless, the difference between them seems not very significant.

Note that FA-GGBS-HMNS based geopolymer paste is a brittle material and thus, under a static loading, it will not have large plastic strain or obvious strain hardening. The reason that it exhibits ductile in the present impact tests, is partly because the effect of high strain rate and partly because the effect of the aspect ratio of the specimens. The fundamental of the SHPB impact test is based on the one-dimensional stress wave propagation theory, in which, ideally, the longitudinal dimension of the specimen should be greater than the sectional dimension of the specimen. However, the longer the specimen, the viscosity effect would be more dominant than the strain rate effect. In the present impact tests, we chosen to use the disk shape, instead of the cylindrical shape, for examining the strain rate effect, which inevitably leads to an increase of the aspect ratio effect. The big difference between a cylinder-shaped specimen and a disk-shaped specimen is that they have different stress states when both of them are only subjected to an axially compressed load. The cylinder-shaped specimen is in a uniaxial-stress state; whereas the disk-shaped specimen is in a three-dimensional stress state with confined stresses from radial and circumferential directions, which can increase the axial compressive load-carrying ability of the disk-shaped specimen. Under impact loading, not only the strain induced confinement but also the lateral inertial force could affect the dynamic failure mechanism of the disk-shaped specimen[23,24]. This explicates how difficulty in carrying out the impact tests of cementitious materials.

The average strain rate of a specimen for a given impact speed can be calculated using Eq.(1). Owing to different diameters in different sets of specimens, the strain rates would be different for specimens with different diameters even for the same impact speed. Note that the diameter of the Hopkinson bars is 40 mm. Thus, in theory, the strain rate calculated for the specimens of diameters 36 mm and 37 mm would be more accurate than that for the specimens of diameter 33 mm. In other words, the dimension and side effect will be slightly larger in the specimens of diameter 33 mm than in those of diameter 36 mm or 37 mm. The effect of strain rate on the ultimate compressive strength of the FA-GGBS-HMNS based GP paste could be described by using the ratio between the dynamic compressive strength and static compressive strength, which is commonly known as the dynamic increase factor (DIF). In literature the DIF has been

used to assess the strain rate sensitivity of cementitious materials[3,25,26,27,28]. In our previous study, the static compressive strength of the FA-GGBS-HMNS based geopolymer pastes (50 mm x 50 mm x 50 mm cubic sample) was found to be about 48.4 MPa[7]. The equivalent static compressive strength of the cylindrical sample thus would be 0.96x48.4=46.5 MPa[29]. By using this equivalent static compressive strength as the normalized factor, we can plot the DIF against the strain rate, which is shown in Figure 8. It is evident from Figure 8 that for specimens with diameters d = 36 mm or 37 mm, DIF increases clearly with the strain rate, which is consistent with what was reported[30] in literature; whereas for specimens with diameter d = 33 mm, the DIF is a little scatter due to their strain rates that were inaccurately calculated because of the side effect and different sectional sizes between the Hopkinson bars and the specimens.

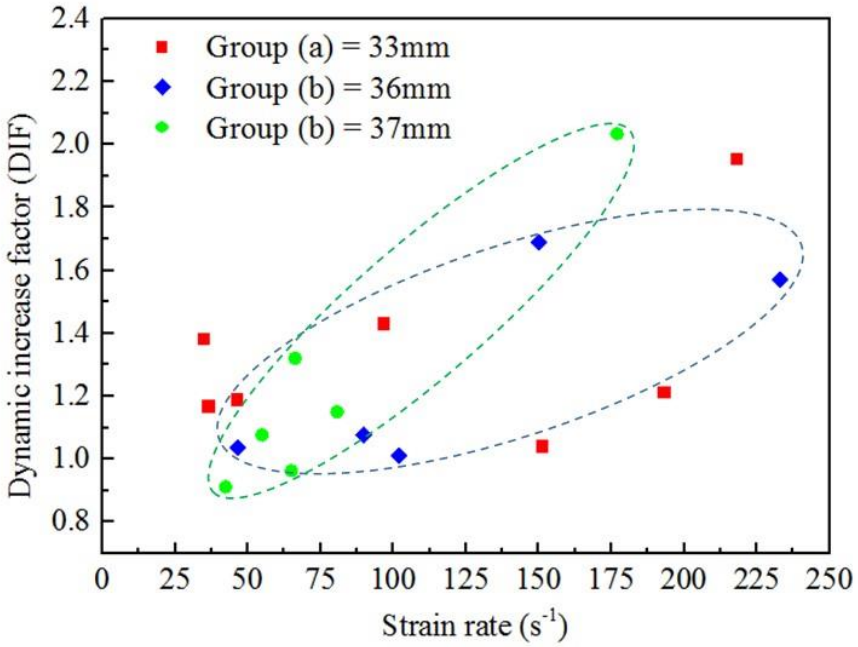

Figure 8. Dynamic increase factor of FA-GGBS-HMNS based geopolymer pastes.

Figure 9 shows three representative failure modes of the FA-GGBS-HMNS based geopolymer paste obtained from three specimens with different strain rates. It is evident from the figure that the impact speed and/or strain rate has a significant influence on the failure mode of the specimen. For the specimen with a low strain rate of 24.1 s^{-1}, the failure mode of the specimen is characterized by several large longitudinal cracks caused by the compressive impact loading, which leads to the specimen split into several large pieces (see Figure 9a). In contrast, for the specimen with a high strain rate of 162 s^{-1}, the specimen was failed by crushing, instead of cracks, which leads to a large number of fine fragments (see Figure 9c). While for the specimen

with a medium strain rate of 83 s^{-1} its failure mode is similar to that of one with low strain rate but has more crushed pieces (see Figure 9b). Chen et al.[31] stated that the cracks in cement paste are mostly straight and long when compared to those in concrete or mortar specimens. In the present impact tests, it was found that when the strain rate is lower than 51.2 s^{-1} the specimens were indeed failed by the straight cracks as shown in Figure 9a. This finding appears to be consistent with what was reported in a recent study, which shows that the cementitious material was failed by crackling for stain rate less than 50 s^{-1}, and by crushing when the strain rate was over 63 s^{-1} [32].

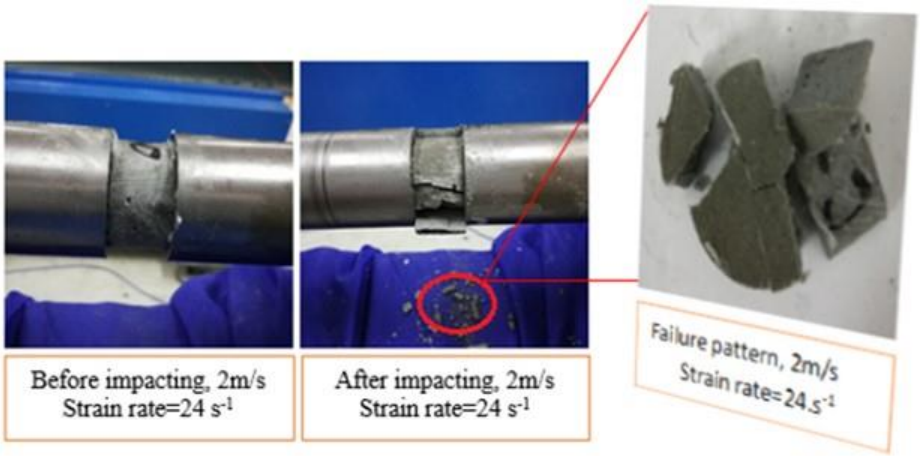

(a)

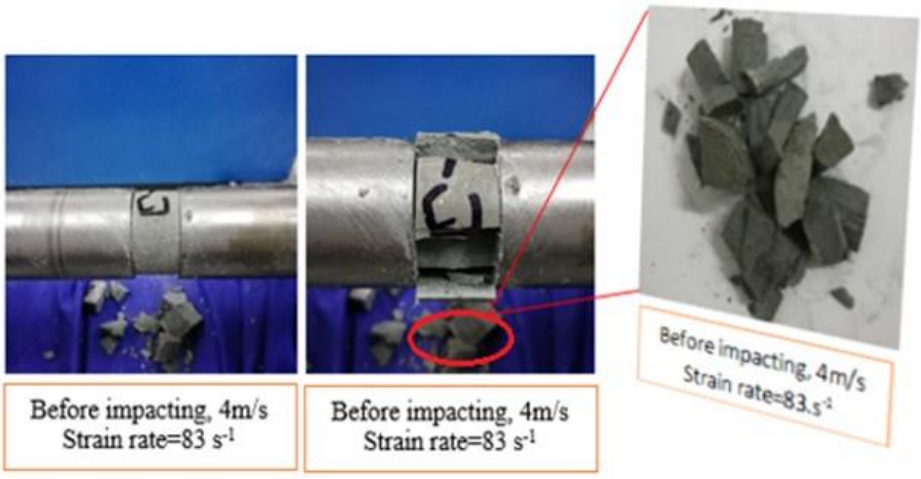

(b)

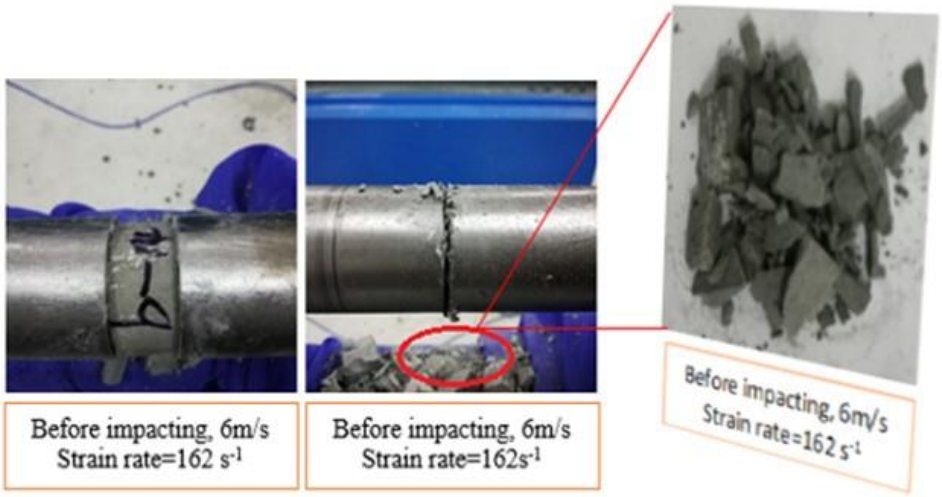

(c)

Figure 9. Failure modes of FA-GGBS-HMNS based geopolymer paste specimens at (a) low strain rate, (b) medium strain rate and (c) high strain rate.

As mentioned above, during the impact the stress wave is transmitted and reflected at the interface between the specimen and incident bar. While the stress wave propagates in the specimen, part of its kinetic energy is dissipated due to the viscosity of the material and the plastic deformation occurred in the specimen. The energy absorbed during the impact by the material is one of the important features for cementitious materials, which has been believed to be influenced by strain rate[25,33]. Figure 10 shows the energy absorbed during the impact for the tested FA-GGBS-HMNS based geopolymer paste specimens. It can be observed from the figure that the energy absorbed by the specimen increases with the strain rate. The increase is quick for low strain rates but tends to be saturated after the strain rate reaches to 130 s^{-1}. For instance, the energy absorbed ranges from 0.49 J to 0.80 J when the strain rate varies from 24.1 s^{-1} to 130 s^{-1}, indicating that the FA-GGBS-HMNS based geopolymer paste has a good level of toughness. An empirically fitted expression for the experimental data shown in Figure 10 is obtained and can be expressed as follows,

$$W_{ab} = 0.306 + 6.5 \times 10^{-3}\dot{\varepsilon} - 2.0 \times 10^{-5}\dot{\varepsilon}^2 \quad (4)$$

where W_{ab} in J is the energy absorbed by the specimen and $\dot{\varepsilon}$ in s^{-1} is the average strain rate.

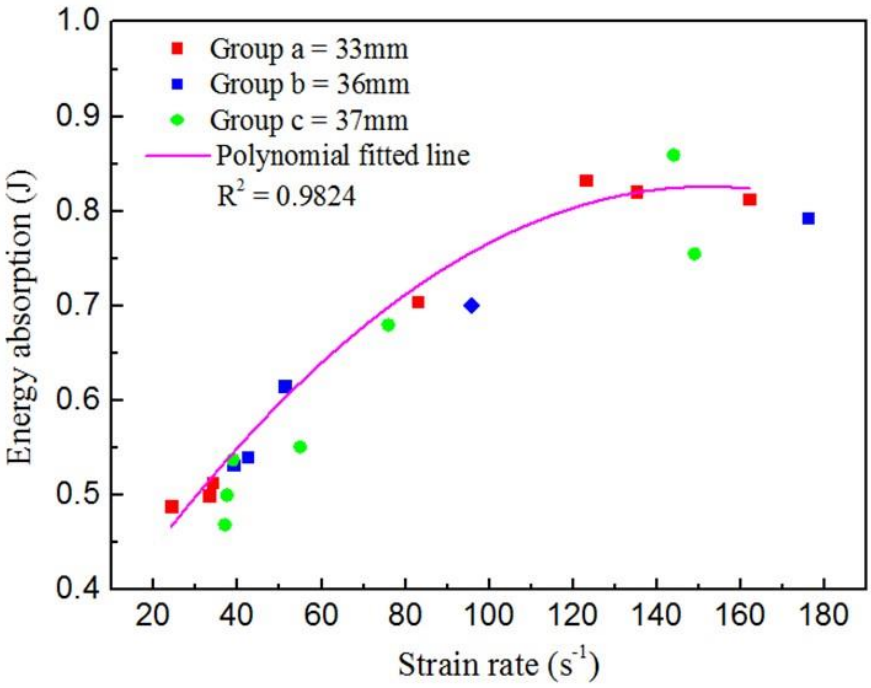

Figure 10. Energy absorption of FA-GGBS-HMNS based geopolymer paste at different strain rates.

5. Conclusions

This paper has presented an experimental investigation on the dynamic mechanical properties of FA-GGBS-HMNS based geopolymer paste under impact loading. The experiments were performed using a 40 mm diameter SHPB apparatus. A total of 27 geopolymer paste specimens with a thickness of 18 mm and three different diameters (33 mm, 36 mm, 37 mm) were tested by using three different impact speeds. From the experimentally obtained results the following conclusions can be drawn:

- The dynamic stress-strain curve of the FA-GGBS-HMNS based geopolymer paste exhibits an initially fast increase almost linearly with the strain, then it has a slow improvement with the increased strain, and finally after the stress reaches to an ultimate value it drops rapidly representing the compression failure.
- The dynamic yield stress of the FA-GGBS-HMNS based geopolymer paste seems not very sensitive to the strain rate; but the dynamic ultimate compressive strength of the FA-

GGBS-HMNS based geopolymer paste is quite sensitive to the strain rate. The higher the strain rate, the larger the dynamic ultimate compressive strength.

- Unlike the static stress-strain curve, the dynamic stress-strain curve of the FA-GGBS-HMNS based geopolymer paste has a clear strain-hardening zone. This ductile behavior is partly due to the dynamic loading and partly due to the dimensional effects of the tested specimens.
- The failure mode of the FA-GGBS-HMNS based geopolymer paste is heavily dependent on the impact speed and the strain rate occurred in the specimen. For low strain rates the failure is mainly due to few large cracks generated in the loading direction; whereas for high strain rates the crushing failure is the dominant failure mode.
- The energy dissipation or the energy absorbed by the material during the impact is found to be dependent on the strain rate. The relationship been the energy absorbed and the strain rate for the FA-GGBS-HMNS based geopolymer paste can be approximately expressed by a quadratic polynomial function.

Acknowledgement - The authors would like to acknowledge the financial support received from the European Commission Research Executive Agency via a Marie Skłodowska-Curie Research and Innovation Staff Exchange project (H2020-MSCA-RISE-2015-PRIGeoC-689857).

References

[1] X. Chen, S. Wu, J. Zhou, *Constr. Build. Mater.* **2013**, *47*, 419.

[2] S. Hentz, F. V. Donzé, L. Daudeville, *Comput. Struct.* **2004**, *82*, 2509.

[3] W. Ren, J. Xu, J. Liu, H. Su, *Ceram. Int.* **2015**, *41*, 11852.

[4] A. Khezrloo, E. Aghaie, M. Tayebi, *J. Aust. Ceram. Soc.* **2018**, *54*, 65.

[5] M. C. G. Juenger, F. Winnefeld, J. L. Provis, J. H. Ideker, *Cem. Concr. Res.* **2011**, *41*, 1232.

[6] B. Singh, G. Ishwarya, M. Gupta, S. K. Bhattacharyya, *Constr. Build. Mater.* **2015**, *85*, 78.

[7] A. Bouaissi, L. Y. Li, M. Mustafa, A. Bakri, Q. Bui, *Constr. Build. Mater.* **2019**, *210*, 198.

[8] L. Xin, J. Y. Xu, W. Li, E. Bai, *Mater. Lett.* **2014**, *124*, 310.

[9] T. Ficker, *Cem. Concr. Res.* **2011**, *41*, 129.

[10] X. Luo, J. Y. Xu, E. L. Bai, W. Li, *Constr. Build. Mater.* **2013**, *48*, 166.

[11] Y. Gao, J. Xu, E. Bai, X. Luo, J. Zhu, L. Nie, *Ceram. Int.* **2015**, *41*, 12901.

[12] S. Wu, X. Chen, J. Zhou, *Constr. Build. Mater.* **2012**, *36*, 448.

[13] B. D. Liu, W. J. Lv, L. Li, P. F. Li, *Constr. Build. Mater.* **2014**, *69*, 133.

[14] P. Rossi, L. Centr, *Mag. Concr. Res.* **1991**, *43*, 53.

[15] D. Zheng, Q. Li, *Eng. Fract. Mech.* **2004**, *71*, 2319.

[16] W. Yao, K. Xia, Y. Liu, Y. Shi, K. Peterson, *Constr. Build. Mater.* **2019**, *202*, 891.

[17] Y. Xu, F. Dai, *Rock Mech. Rock Eng.* **2018**, *51*, 747.

[18] B. T. Tang, L. E. Malvern, D. A. Jenkins, *J. Eng. Mech* **1992**, *118*, 108.

[19] M. Khandelwal, P. G. Ranjith, Z. Pan, J. G. Sanjayan, *Arab. J. Geosci.* **2013**, *6*, 2383.

[20] K. N. Feng, D. Ruan, Z. Pan, F. Collins, Y. Bai, C. M. Wang, W. H. Duan, *Mater. Struct.* **2015**, *48*, 671.

[21] O. S. Lee, M. S. Kim, *Nucl. Eng. Des.* **2003**, *226*, 119.

[22] M. M. Al-Mousawi, S. R. Reid, W. F. Deans, *Proc. Instn. Mech. Engrs. (Part C)* **1998**, 211, 273.

[23] Y. Hao, H. Hao, G. P. Jiang, Y. Zhou, *Cem. Concr. Res.* **2013**, *52*, 63.

[24] M. Zhang, H. J. Wu, Q. M. Li, F. L. Huang, *Int. J. Impact Eng.* **2009**, *36*, 1327.

[25] H. Su, J. Xu, *Constr. Build. Mater.* **2013**, *45*, 306.

[26] G. U. O. Yang, X. Chen, W. Xuan, Y. Chen, *Sādhanā* **2018**, *43*, 165.

[27] Q. Fu, D. Niu, J. Zhang, D. Huang, Y. Wang, *Arch. Civ. Mech. Eng.* **2018**, *18*, 914.

[28] M. Zaheer, N. Khan, Y. Hao, H. Hao, A. Shaikh, *Cem. Concr. Compos.* **2019**, *104*, 103343.

[29] B. Graybeal, M. Davis, *ACI Mater. J.* **2008**, 603.

[30] J. W. Tedesco, J. C. Powells, C. A. Ross, M. L. Hughes, *Comput. Struct.* **1997**, *64*, 1053.

[31] X. Chen, S. Wu, J. Zhou, *Constr. Build. Mater.* **2013**, *47*, 419.

[32] S. Cao, E. Yilmaz, W. Song, *Constr. Build. Mater.* **2018**, *186*, 892.

[33] D. J. Kim, K. Sirijaroonchai, S. El-tawil, A. E. Naaman, *Int. J. Impact Eng.* **2010**, *37*, 141.